small structures
www.small-structures.com

Post-Synthetic Graphitization and Photoluminescence Tuning of Carbon Dots from *L*-Glutamic Acid

Andrés Ferrer-Ruiz, Laura Rodríguez-Pérez, Nazario Martín, and María Ángeles Herranz**

Carbon dots are promising luminescent nanostructures. Their availability, based on inexpensive precursors and their intrinsic fluorescent nature, place them as potential choices against traditional quantum dots in some applications. However, the carbon dots nature is nowadays not well defined and understood. They are usually hybrid nanomaterials in terms of structure and composition, which hinders the knowledge of their photoluminescence mechanisms. Herein, the solvent-free pyrolysis of *L*-glutamic acid by microwave synthesis leads to an incomplete graphitization of the precursor resulting in loose polymer-like nanohybrids. Further experiments confirm that these carbon dots (CD) can be crosslinked and graphitized in a second heating step when using temperatures above 160 °C, reaching a plateau of graphitization over 200 °C. An exhaustive analysis by thermogravimetric analysis, Raman and X-ray photoelectron spectroscopy highlights the structural changes undergo from 140 to 200 °C, where an increase of stability is observed due to the graphitization process. The condensation and decarboxylation reactions with loss of hydrophilic functional groups like amine and carboxylic acids explain the formation of sp^2 domains and the concomitant loss of solubility. The annealed CD exhibit a broader and slightly red-shifted emission band, with lower emission quantum yields, when compared to the initial nanohybrids.

1. Introduction

Carbon-based materials are crucial to the advancement of materials science. Well-established forms, like activated carbon and carbon black, and traditional types, such as carbon fibers and graphite, have long been essential in the chemical industry. In recent decades, innovative carbon nanomaterials, including fullerenes, carbon nanotubes, and graphene have also become prominent. These materials are widely studied and utilized across chemistry, materials science, and other interdisciplinary fields, largely due to their environmental benefits.[1] However, conventional macroscopic carbon materials often lack the suitable band gap required to function as effective fluorescent probes. This is where fluorescence nanoscale carbon particles in the range of 1–10 nm, the so-called carbon dots (CD), come into play emerging as a promising new member of the carbon family.[2] In the last years, they are positioning as an alternative to metal-based semiconductor quantum dots (SQD)[3] for their exceptional and tunable photoluminescence (PL), with low toxicity, good biocompatibility, and cost-effectiveness.[4]

Since the seminal report of Sun et al. in 2006,[5] and attending to their nature, quantum confinement, and crystalline structure, a variety of terms have emerged to describe different categories of CD.[6] The samples derived from the thermal treatment of various organic materials from amino acids to biomass,[7,8] can be broadly classified as carbon quantum dots (CQD) and carbon nanodots (CND).[9] CQD possess a carbon core with certain degree of crystallinity and their fluorescence shows quantum confined effects, while CND usually possess a carbonized core structure without obvious crystallinity and their fluorescence does not show any quantum confined effects. To regulate CD properties the surface capping should be carefully considered as well. It is usually populated with abundant and random defects caused by peripheral organic functionalities dominated by amines, alcohols, and carboxylic acids.[10] These functionalities make CD to present a hydrophilic character, compatible with reactions in aqueous media, and also enhanced PL in comparison with naked carbon nanoparticles.[5]

The synthesis and derivatization of CD has been explored to developed materials for diverse applications, including biomedicine,[11] catalysis,[12] and optoelectronic devices.[13] Within the reported procedures, thermal or hydrothermal approaches from small organic precursors are particularly versatile. They enable the exploration of several core/surface relationships and allow

A. Ferrer-Ruiz, L. Rodríguez-Pérez, N. Martín, M. Á. Herranz
Organic Chemistry Department
Faculty of Chemical Sciences
Complutense University of Madrid
Av. Complutense s/n, 28040 Madrid, Spain
E-mail: nazmar@ucm.es; maherran@quim.ucm.es

N. Martín
IMDEA Nanoscience
Ciudad Universitaria de Cantoblanco
C/ Faraday 9, 28049 Madrid, Spain

The ORCID identification number(s) for the author(s) of this article can be found under https://doi.org/10.1002/sstr.202400532.

DOI: 10.1002/sstr.202400532

the optimization and tuning of properties. The primary advantage of these methods lies in its simplicity and speed, often allowing for a "one-pot" processing approach that typically takes from a few minutes to hours. During the treatment under high pressure or elevated temperature the organic precursors tend to dehydrate and crosslink to produce a fluorescent material. The final structure and properties of CD are deeply affected by the choice of precursors and synthetic conditions, including decomposition temperature, treatment duration, and the choice of solvent.[7,14] Particularly, heteroatom doping is a common strategy to optimize the optoelectronic properties of CD and nitrogen has been extensively used to raise the electron density and the quantum yield (QY) of CD.[2] However, one of the main drawbacks in the field is the development of reproducible purification strategies, which are often inadequate, poorly substantiated, or entirely absent, resulting in misconceptions about the nature and properties of these materials.[15] Several researchers have already alluded to the fact that during the bottom-up synthesis, molecular fluorophores (potentially oligomeric or polymeric in nature) are formed as by-products, which account for most of the emission from these CD composite samples.[16] For moving forward, rigorous and consistent purification steps will need to be uniformly implemented to guarantee the reproducibility of the properties and, the control of the functionalities introduced on the surface of CD for successful post-synthetic modifications.

With this motivation in mind, here, we report the pyrolytic synthesis of CD from an organic precursor, *L*-glutamic acid, in a microwave reactor. Subsequent experiments have been performed to understand the graphitization process undergone by these CD once subjected to an annealing treatment and the variations observed on their structure and optical properties. In this article, we use the term CND to describe all the types of CD produced, ever since they are carbon-based quasi-spherical particles that could be described as nanocarbon polymeric hybrids with different contents of sp^3 carbon and sp^2 domains.[17]

2. Results and Discussion

2.1. Pyrolytic Synthesis and Characterization of *L*-Glutamic Acid CND

CND have been synthesized via the pyrolysis of *L*-glutamic acid in a microwave reactor. Specifically, *L*-glutamic acid was placed in a microwave tube and heated to its decomposition temperature of 210 °C for 10 min. The resulting dark brown solid indicates the successful formation of CND_{aGlu} (**Scheme 1**). Subsequently, larger aggregates were removed through filtration, and any remaining starting material in the obtained solution was eliminated via precipitation to yield a brown solid with a 34% w/w yield (more details in the experimental section).

The investigation of the spectroscopic features of this new nanomaterial (**Figure 1**) reveals in the UV-Vis spectrum of CND_{aGlu} in MeOH an absorption maximum at 215 nm, along with an additional band at 334 nm, attributed to π–π* and n–π* transitions, respectively.[18] In terms of PL properties, upon light excitation ($\lambda_{exc} = 350$ nm) the as-prepared CND_{aGlu} display a strong emission at 430 nm responsible of the blue emission visible to the naked eye (Figure 1b).

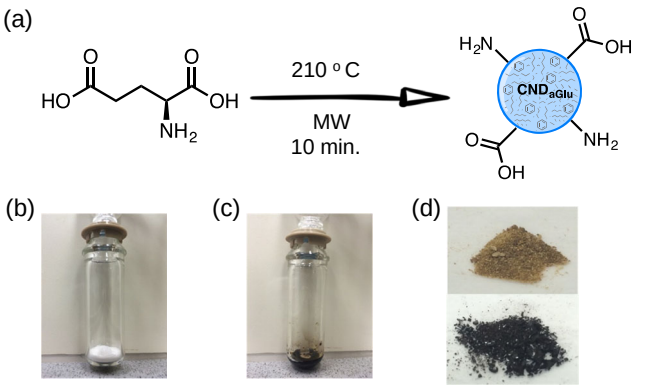

Scheme 1. a) Schematic representation of CND_{aGlu} synthesis. b) *L*-glutamic acid before the microwave treatment. c) Reaction crude obtained after microwave reaction. d) CND_{aGlu} powder obtained after purification (upper) and after 72 h of thermal treatment at 220 °C in an oven (see discussion in section 2.2).

Conclusion of the strong fluorescent homogeneity could be drawn from transmission electron microscopy (TEM), where rather uniform and monodisperse CND_{aGlu} with average diameters of 1.4 ± 0.2 nm can be found (Figure 1c,d). Complementary investigations by atomic force microscopy (AFM) offer a similar picture of the sample, displaying individual objects of average heights of 1.6 ± 0.5 nm together with small aggregates (Figure S1, Supporting Information).

According to prior reports, mass spectrometry presents a valuable method for acquiring information regarding the size and composition of the sample.[19] MALDI-TOF analysis showed a molecular weight distribution, as expected from the random combination of various atoms, centered around 2000 Da (Figure S2b, Supporting Information). Below this molecular weight, only small oligomers were identified, and no free *L*-glutamic acid was detected (Figure S2a, Supporting Information).

To gain structural insights, X-ray photoelectron spectroscopy (XPS) and Fourier-transform infrared (FTIR) experiments were conducted. The XPS survey spectra, depicted in **Figure 2**, showed three primary features at 284.6, 399.6, and 531.6 eV corresponding to the C 1s, N 1s, and O 1s core-level contributions of CND_{aGlu}, as it was anticipated. Deconvolution of the C 1s core-level peak displays four species with binding energies of 284.8 eV (C—C/C═C), 285.7 eV (C—O/C—N), 286.4 eV (C═O), and 288.1 eV (O—C═O). Notably, it is important to mention the lack of the shake-up fingerprint, characteristic contribution for graphitic systems. Additionally, the deconvolution of the N 1s and O 1s peaks provided binding energies consistent with carboxylic acids, amides, and free amines present in the CND_{aGlu} structure. Finally, and as expected, the content of graphitic-N is quite low due to the limited number of sp^2 carbons in the CND_{aGlu} framework. Additional proof for these functional groups came from FTIR spectroscopy. In Figure S3 (Supporting Information) typical stretching vibration modes of C═O, C—N, and C—O are noted at 1725–1637, 1460–1383, and 1241–1085 cm^{-1}, respectively. In addition, the stretching vibrations of O—H and N—H evolve around 3300 cm^{-1}, while aliphatic C—H bond stretching vibrations are discernible at 2925–2833 cm^{-1}. However, the characteristic C═C stretching

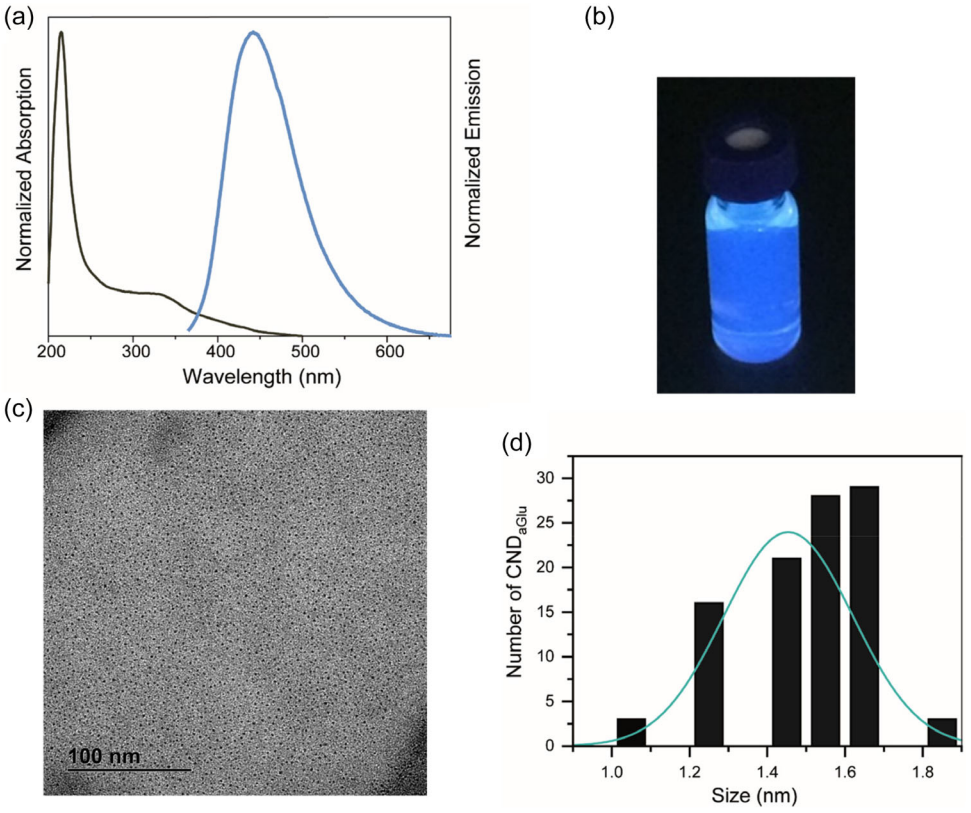

Figure 1. a) Normalized UV-Vis absorption spectrum (black) and emission spectrum under 350 nm excitation wavelength (blue) of CND_{aGlu} in MeOH. b) CND_{aGlu} solution in MeOH under 365 nm light irradiation. c) TEM image of CND_{aGlu}. d) Size distribution histogram with a curve fit of the data using a Gaussian model. Average height: 1.4 ± 0.2 nm.

vibration is only observed in the form of a small shoulder included in the band of the C═O groups.

Complementary information regarding the nature of the sample was obtained through X-ray diffraction (XRD) and Raman spectroscopy. The diffractogram of CND_{aGlu} consists of several distinct peaks, indicating a crystalline polymeric phase rather than an amorphous graphitic structure (Figure S4, Supporting Information). To ensure that these peaks were not attributable to residual *L*-glutamic acid, the diffractogram of CND_{aGlu} was compared with that of *L*-glutamic acid, revealing no coinciding diffraction peaks.[20] This analysis confirms the synthesis of a novel nanomaterial with a crystalline phase that has not been previously reported. Raman spectroscopy further supports these findings discussed atop, as no features characteristic of graphitic systems (such as the D and G bands) were observed for CND_{aGlu}; only the typical fluorescence background was recorded during the experiments. These characteristics are indicative of polymeric-like CDs, where incomplete carbonization may lead to the formation of nanohybrid structures rather than graphitic forms.[21]

2.2. Graphitization Study

Considering the structural characterization performed on the CND_{aGlu} samples, the methodology employed in this study appears to yield incomplete carbonization, resulting in polymer-type materials with a predominant ratio of sp^3 to sp^2 carbon domains, as well as a variety of polar oxygenated and nitrogenated functionalities. Consequently, we aimed to investigate whether post-treatment carbonization could enhance the degree of sp^2 domains. In these experiments, several CND_{aGlu} samples were subjected to heating in an oven for 72 h at varying temperatures ranging from 100 to 220 °C, followed by further characterization. To clearly differentiate the samples, the as-prepared CND_{aGlu} were labeled as $CND_{aGlu\ Ini}$, while the heated samples were designated according to their respective heating temperatures; for instance, the CND heated to 100 °C were referred to as $CND_{aGlu\ 100}$, and so forth.

The first property examined following the annealing experiments was the thermal stability of each sample, as assessed by thermogravimetric analysis (TGA) (**Figure 3**, left). Up to 140 °C, no significant changes in thermal stability were observed compared to the $CND_{aGlu\ Ini}$ reference material. However, beyond 140 °C, the material appears to initiate a graphitization process, leading to an increase in thermal stability. This process reaches its maximum thermal stability at 220 °C (Figure S5, Supporting Information), with the primary weight loss occurring around 400 °C, which is nearly 150 °C higher than that observed for $CND_{aGlu\ Ini}$.

Additionally, XRD analysis provided further insights into the structural evolution of $CND_{aGlu\ Ini}$ after each heating step.

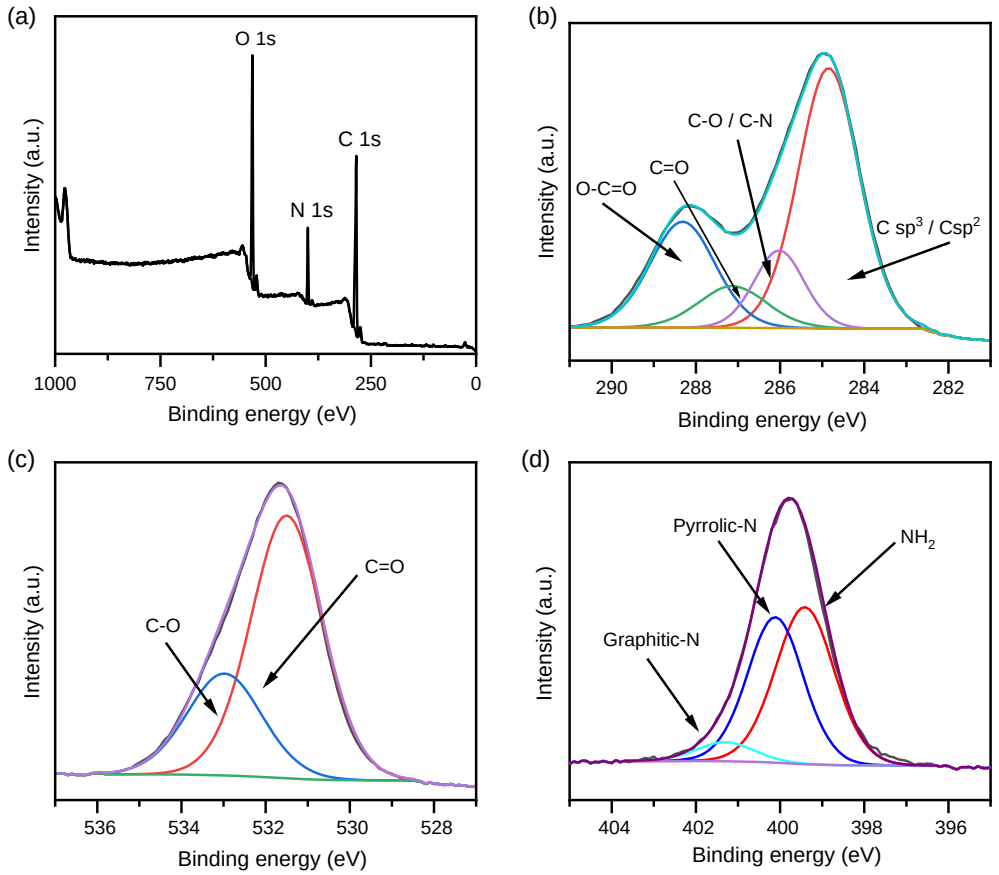

Figure 2. XPS analysis of CND_{aGlu}: a) Survey spectrum. b) C 1s component deconvolution. c) O 1s component deconvolution. d) N 1s component deconvolution.

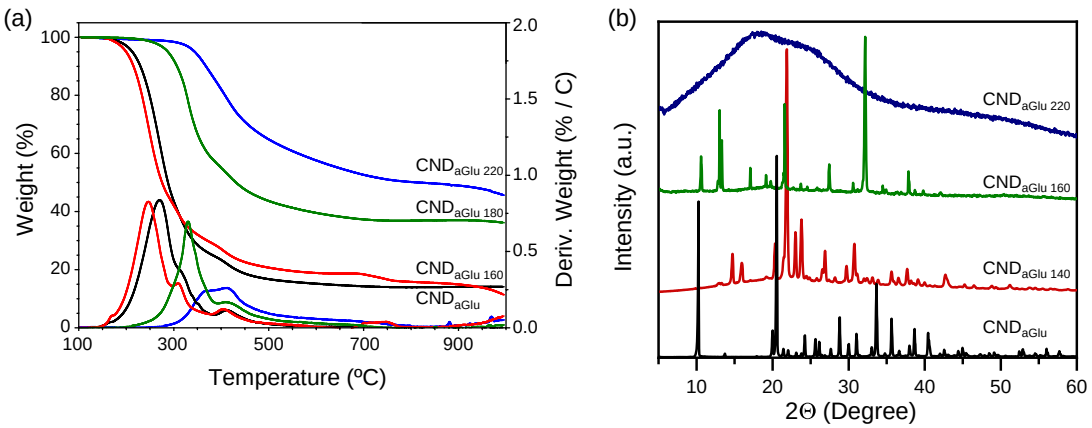

Figure 3. a) TGA and first derivative under inert conditions of $CND_{aGlu\ Ini}$, and samples heated in an oven for 72 h at temperatures of 160, 180, and 220 °C. b) XRD diffractograms of $CND_{aGlu\ Ini}$, and samples heated in an oven for 72 h at temperatures of 140, 160, and 220 °C.

The XRD patterns indicate a transition from crystalline materials, characterized by distinct diffraction peaks (for Ini, 140, and 160 °C), to a broad diffraction peak at 220 °C, indicative of an amorphous graphitic structure (Figure 3b). Consequently, various crystalline phases are derived from the $CND_{aGlu\ Ini}$ structure up to 160 °C, at which point a rapid graphitization occurs, generating a new amorphous lattice similar to that observed in graphite-based materials.[22,23]

Raman spectra of the solid materials were recorded by using an excitation wavelength of 785 nm (**Figure 4**). This excitation wavelength falls within the long-wavelength tail of the fluorescence spectra of the samples, reducing interference from strong

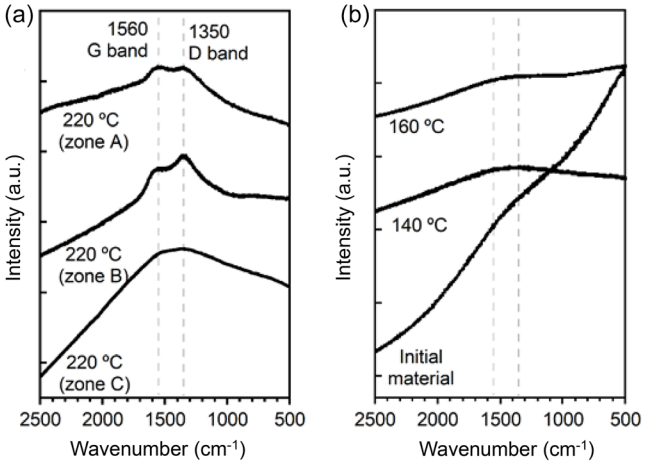

Figure 4. Raman spectra of $CND_{aGlu\ Ini}$, $CND_{aGlu\ 140}$, $CND_{aGlu\ 160}$, and $CND_{aGlu\ 220}$, obtained with a laser excitation wavelength of 785 nm.

PL, which is common when excitations at 532 or 633 nm are used. Despite these precautions, Raman spectra remain unresolved for samples treated at temperatures below 220 °C, as shown in Figure 4, where a typical fluorescence background is obtained. In contrast, for the sample obtained at 220 °C, the Raman spectrum is resolved and presents the typical two bands pattern at 1300–1350 and at 1560–1600 cm^{-1}, which correspond to the characteristic D and G Raman bands of graphitic materials, respectively. However, at this temperature, the solid sample does not uniformly graphitize, as it is seen in the spectra taken in zones of the sample with different brightness. The starting material, along with samples annealed at 140 and 160 °C, exhibits a spectral background without vibrational resolution, consistent with their strong fluorescence. Nonetheless, the forms of the D and G bands start to get profiled in these samples at intermediate temperatures.

XPS provided further insights into the graphitization process of $CND_{aGlu\ Ini}$. Table S1 (Supporting Information) presents the elemental composition and deconvolution data for $CND_{aGlu\ Ini}$, $CND_{aGlu\ 160}$, and $CND_{aGlu\ 220}$. The compositional analysis indicates an increase in carbon content during the graphitization process, accompanied by a reduction in oxygen content. Unlike carbon and oxygen, the nitrogen distribution experiences only a marginal decrease as the graphitization progresses. This can be accounted for the decarboxylation of carboxylic acids during thermal treatment, which promotes the formation of new sp^2 carbon structures, extending the π-conjugated network. By this reason, the content of oxygen would decrease, and the content of carbon would increase, as the obtained results show.

Looking inside the deconvolution of the C 1s core-level of the three samples, it is remarkable the increase of the C—C/C=C component, alongside a corresponding reduction in the O—C=O (carboxylic acid) component in samples subjected to higher temperatures (**Figure 5** and Table S1, Supporting Information). The ratio of sp^2 to sp^3 carbon can be determined by analyzing the C 1s spectrum of samples $CND_{aGlu\ 160}$ and $CND_{aGlu\ 220}$, as graphitization progress the percentage of sp^2 increases from 7.2% for $CND_{aGlu\ 160}$ to 27% for $CND_{aGlu\ 220}$. Moreover, in these samples it was also discerned the presence of the distinctive π–π* shake-up band of graphitic structures,[24] confirming the enhancement of sp^2 hybridization with increasing annealing temperature.

Moving to the deconvolution of the N 1s core-level contribution, the nitrogen doping species (pyridinic, pyrrolic, and graphitic) are identified and quantified from the XPS spectra (Table S1, Supporting Information) with a noticeable raise in the graphitic-N species as the annealing temperature increases, with the highest concentration observed in $CND_{aGlu\ 220}$. Finally, in the deconvolution of the O 1s, the drop in the C=O content, accompanied with the raise of the C—O content, is consistent with the trends observed for the C 1s core-level contribution (further supported by FTIR analysis discussed below).

The different functional groups present in the CND_{aGlu} samples were characterized using FTIR and NMR spectroscopies. The FTIR spectra for the initial sample and the sample heated to 140 °C exhibit notable similarities (**Figure 6**). Characteristic peaks at 1723 cm^{-1} and 1635 cm^{-1}, corresponding to the stretching vibrations of carboxylic acid (C=O) and amide (C=O) groups, are evident. Additionally, the broad absorption band spanning 3000–3700 cm^{-1} can be attributed to the O—H stretching vibrations of carboxylic acids and the N—H stretching vibrations of amide groups. The intense peak at 3304 cm^{-1}, observed in both

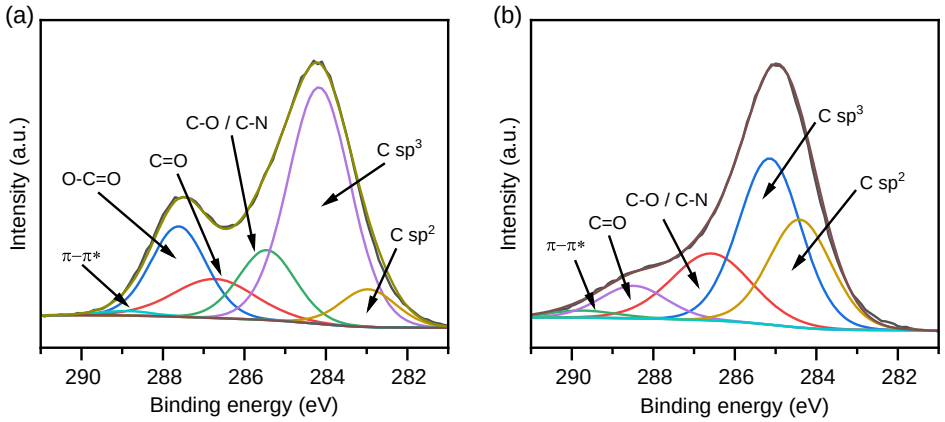

Figure 5. C 1s component deconvolution of the XPS of: a) $CND_{aGlu\ 160}$ and b) $CND_{aGlu\ 220}$.

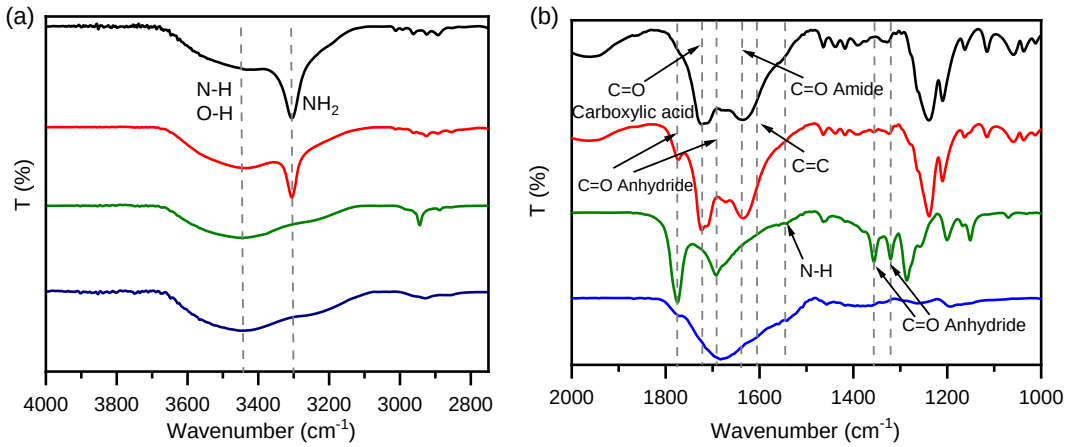

Figure 6. FTIR spectra of $CND_{aGlu\ Ini}$ (black), $CND_{aGlu\ 140}$ (red), $CND_{aGlu\ 160}$ (green), and $CND_{aGlu\ 220}$ (blue). a) From 4000 to 2750 cm^{-1}. b) From 2000 to 1000 cm^{-1}.

spectra, confirms the presence of primary amine groups. Moving to the next sample (160 °C) several changes are observed. On the one hand, two new peaks appear at 1775 and 1692 cm^{-1}, which could be the symmetric and asymmetric C═O stretching modes of anhydride groups. The presence of these groups should be a consequence of a condensation process between free carboxylic acids of the CND. This hypothesis is further supported by the appearance of new peaks at 1355 and 1314 cm^{-1}, which nicely correspond to the symmetric and asymmetric C—O stretching modes of the anhydride groups. On the other hand, the peak associated with free amine groups at 3304 cm^{-1} completely disappears at 160 °C, indicating the loss of amine functionality. These changes imply that the loss of carboxylic acid and amine groups are the driving force for the graphitization of the CND surface leading to the introduction of sp^2-hybridized carbon atoms, thus increasing its thermal stability, as corroborated in the TGA analysis.

In accordance with this observation, the small peak between 1550 and 1600 cm^{-1} is assigned to the newly formed C═C stretching bands.[25] Finally, for the sample heated at 220 °C, very few vibration modes are detected, the most prominent feature being a broad absorption centered at 1683 cm^{-1}, resulting from the superposition of C═O stretching vibrations from anhydrides, amides, and residual carboxylic acids (Figure S6, Supporting Information). Furthermore, it also contains a shoulder due to the C═C stretching bands present in the CND. The significant reduction of bands in this spectrum can be rationalized as a consequence of the significant increase in sp^2 carbon content, indicating the material's transition toward a more graphene-like structure.

In the NMR experiments, in both ^1H and ^{13}C-NMR spectra, no noticeable changes were detected in the registered resonance signals up to 160 °C. However, at this temperature, initial evidence of graphitization began to emerge (Figure S7, Supporting Information). Above 160 °C new signals were discerned in the aliphatic region (highlighted in red) of the spectra but, more important, new features raised up in the aromatic region (highlighted in blue) as a result of the graphitization process which led to the formation of new sp^2 carbons. The carbon signals in the 150–165 ppm range show a distinct upshift, which can be attributed to the influence of electron-withdrawing functional groups in the local chemical environment. Furthermore, it is important to mention the emergence of new signals associated with the formation of additional carboxylic and amide groups.

In addition to the structural transformations, morphological changes were also noticed by AFM microscopy. The most notable comparison is that observed between $CND_{aGlu\ Ini}$ (Figure S1, Supporting Information) and the sample annealed at 220 °C (Figure S8, Supporting Information). The latter exhibits a more heterogeneous distribution of nanoparticles. AFM statistical analysis of the heights of 100 nanoparticles from the $CND_{aGlu\ 220}$ sample yielded an average height of 2.1 ± 0.6 nm, slightly higher than the 1.6 ± 0.5 nm average height measured for $CND_{aGlu\ Ini}$. This increase in height can be attributed to particle growth during annealing, along with the increased sp^2 carbon content resulting from the condensation of polymer-like chains. In this process, the loose of functional groups such as amines and carboxylic acids takes places. Furthermore, MALDI-TOF experiments also confirmed that through the annealing processes, the molecular weight of the samples slightly increases. Figure S9 (Supporting Information) shows the MALDI-TOF spectra of $CND_{aGlu\ 220}$ which present a polydisperse profile with most of the population located around 2500 Da, 500 Da above that observed for $CND_{aGlu\ Ini}$ (2000 Da).

The optical absorption in the visible and near-UV spectral regions also plays a critical role in ensuring the accuracy of analyses by helping to rule out interference from molecular dyes or chromophore contaminants in the samples of CND. Nanoscale carbon entities produced by carbonization of organic molecules exhibit quite stable absorption characteristics across a broad spectral range (≈350 to 800 nm), with minimal variation even with surface modifications or doping.[7] This stability is analogous to that observed in other nanoscale carbon materials, such as multiwalled carbon nanotubes, due to their similar electronic transition behaviors.[14,26] Specifically, CND are effective in photon-harvesting in the short-wavelength region of the UV-Vis spectra due to their structural features. The origin of this absorption stems from a variety of π–π* (C═C) transitions in the UV-Vis region (260–320 nm) with a tail extending into the visible

range.[21,27] In some cases, it is also observed a shoulder peak in the range of 270–390 nm which can be ascribed to n–π* transitions of C═O bonds.[28] In this context, the UV-Vis spectra shown in Figure 1 and Figure S10 (Supporting Information) demonstrate the characteristic absorption features of $CND_{aGlu\ Ini}$ with distinct π–π* (C═C) and n–π* (C═O) transitions arising from their sp^2 nanodomains and surface carboxyl groups, as mentioned earlier. However, CND exhibit significantly enhanced absorption, particularly due to the increased number of π–π* transitions, with a pronounced tail in the visible region for $CND_{aGlu\ 220}$. The loss of surface carboxyl functionalities during the annealing process is evidenced by the decrease of the n–π* transition bands in the spectra of annealed samples $CND_{aGlu\ 160}$ and $CND_{aGlu\ 220}$.

Interestingly, all the CND synthesized exhibit fluorescent, with the emission color shifting from blue to yellowish as the degree of graphitization increases (**Figure 7**a). The emission of selected CND_{aGlu} samples under 365 nm excitation wavelength is shown in Figure 7b. As the annealing temperature increases, the emission bands broaden, accompanied by a slight red-shift in the maximum emission peak. This broadening of the emission profile closely resembles that observed in graphene quantum dots (GQDs), which matches the previous evidence of the graphitization of the samples.[26]

Excitation-dependent emission studies reveal a consistent trend for samples heated up to 180 °C: a red-shift in the emission peak as the excitation wavelength increases, accompanied by a decrease in fluorescence intensity (Figure 7c). However, in samples heated above 180 °C, while a red-shift is still observed, the fluorescence intensity increases with longer excitation wavelengths (Figure 7d). Furthermore, the fluorescence quantum yield of CND decreased to 4.5% ($CND_{aGlu\ 180}$) and 2.2% ($CND_{aGlu\ 220}$) from a 13.8% of $CND_{aGlu\ Ini}$. These findings are preliminarily consistent with PL mechanisms involving trap states and assembled individual emitters of different sizes, although further investigations are ongoing to confirm these mechanisms.[6,28]

Finally, it is important to note that the graphitization of CND_{aGlu} not only influences its optical properties but also significantly impact its solubility in water. As the graphitization process progresses, the solubility of CND_{aGlu} in aqueous media markedly decreases due to the loss of hydrophilic functional groups, such as amines and carboxylic acids, through condensation and decarboxylation reactions, which promote the formation of sp^2 carbon domains (Figure S11, Supporting Information). Samples subjected to annealing above 180 °C become nearly insoluble in water, in contrast to those heated to lower temperatures. Therefore, during the synthesis of these nanomaterials, it

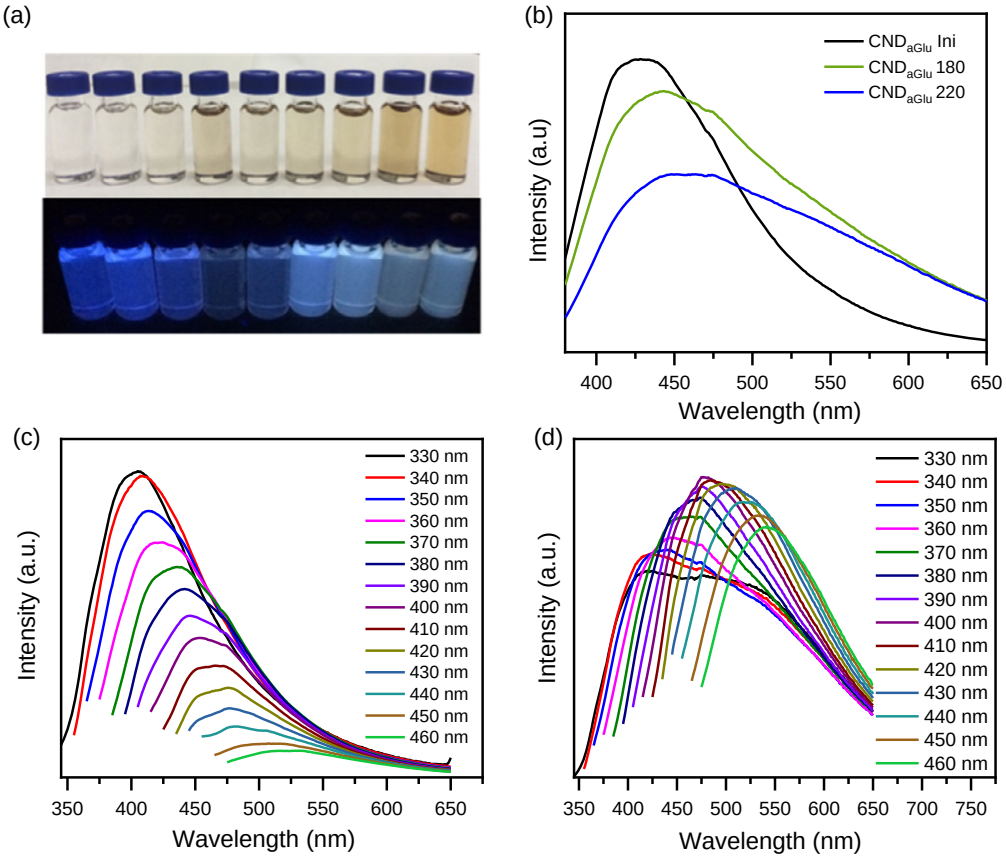

Figure 7. a) Top: 0.1 mg mL^{-1} solutions in DMSO of CND_{aGlu}, going from the initial sample (left) to samples heated at 100, 120, 140, 150, 160, 180, 200, and 220 °C (right). Bottom: The same solutions under 365 nm illumination. b) Emission spectra of $CND_{aGlu\ Ini}$ and the samples heated at 180 and 220 °C in DMSO under 365 nm light irradiation. c) Emission spectra of $CND_{aGlu\ Ini}$ in DMSO at different wavelengths. d) Emission spectra of $CND_{aGlu\ 220}$ in DMSO at different wavelengths.

is crucial to balance the degree of graphitization with the desired solubility features.

3. Conclusion

In summary, CND have efficiently been produced by a bottom-up methodology using microwave-assisted pyrolysis of *L*-glutamic acid. The obtained CND_{aGlu} present quasi-spherical shapes with average heights of 1.6 ± 0.5 nm with a blue-shifted and narrow emission band. However, CND_{aGlu} exhibited a polymeric nature with a structure composed with mostly sp^3 domains. This fact was confirmed from the observed crystalline polymeric phase in XRD experiments, the lack of π–π shake-up contributions in XPS and the absence of graphitic features in Raman experiments. For that reason, a post-treatment carbonization was performed with the aim of obtaining a higher degree of sp^2 domains. These experiments confirmed that it is possible to induce some graphitization in CND_{aGlu} samples in a second heating step when using temperatures above 160 °C, reaching a limit in the graphitization over 200 °C. In this range of temperatures, an increase of the stability in TGA, a graphitic profile (D and G bands) in the Raman spectra, and an increase in the C═C and graphitic-N components in the XPS were observed. Besides the structural changes, CND_{aGlu} subjected to thermal annealing with increasing temperatures, showed a broad emission band, which is slightly red-shifted when compared to the starting CND_{aGlu}. The increase of temperature in the annealing process also influences the fluorescence quantum yields of the resulting materials, which decrease as samples graphitized. Finally, the CND_{aGlu} solubility in water tended to decrease significantly due to the loss of hydrophilic functional groups, namely amines and/or carboxylic acids, through condensation and/or decarboxylation processes, which trigger the formation of new sp^2 graphitized domains.

This detailed study on the effect of temperature on fundamental properties, namely fluorescence, of CND should improve the control on the nature of these fascinating and ease to prepare carbon-based nanomaterials, thus helping to better designing their properties at will.

4. Experimental Section

Materials and Methods: Organic solvents and reagents used in this work were purchased from commercial suppliers and used without further purification, unless stated otherwise. Vacuum filtrations of CND materials were carried out with polytetrafluoroethylene (PTFE) (pore size = 0.1 µm, Φ = 47 cm) membrane.

Thermogravimetric Analyses (TGA): Were carried out with a thermobalance TA-TGA-Q-500 under N_2. The sample (≈0.5 mg) was introduced inside a platinum crucible and equilibrated at 90 °C followed by a 10 °C min^{-1} ramp between 90 and 1000 °C.

Proton Nuclear Magnetic Resonance (^{1}H-NMR) Spectra: Were recorded on a Bruker AVIII-700 at 298 K, using partially deuterated solvents as internal standards. Chemical shifts (δ) are expressed in ppm and are referred to the residual peak of the solvent. Spin multiplicities are reported as singlet (s), doublet (d), triplet (t), quartet (q), multiplet (m), and broad (br), with proton–proton coupling constants (J) given in Hz.

Mass Spectra: MALDI-TOF spectra were determined on a Bruker Autoflex instrument.

FTIR spectra were recorded in solid on a Bruker TENSOR 27 (ATR device, 4000–550 cm^{-1}), with a resolution of 1 cm^{-1}, and in pellets of dispersed samples of the corresponding materials in dried KBr (spectral range was 4000–400 cm^{-1}) with a resolution of 1 cm^{-1}.

Raman Measurements: Excitation wavelengths of 532, 633 and 785 nm were used in an Invia Reflex Raman RENISHAW microscope.

Optical Measurements: UV-Vis-NIR Spectra were recorded in a UV-3600 Shimadzu Spectrophotometer using 1 cm quartz cuvettes. A Horiba Jobin Yvon Fluoromax 3 spectrometer was used for the steady state fluorescence measurements. By recording the S/R-channel the fluorescence spectra are corrected with respect to the lamp spectrum. The integration time was set to 0.1 s, while the entrance and exit slits of excitation and emission monochromator were set to 2 nm. All measurements were performed in 10 × 10 mm quartz cuvettes. The software FluorEscence was used for data evaluation. The quantum yields were obtained in a PicoQuant FluoTime 300 instrument, by a relative method using quinine sulfate (QY = 55% in 0.5 M H_2SO_4), adjusting the optical absorbance to 0.1 at 373 nm and integrating the fluorescence intensity between 380 and 840 nm.

Transmission Electron Microscopy (TEM): Micrographs were obtained using a JEOL JEM 1400 microscope operating at 120 kV. The samples were dispersed in DMSO and dropped onto a holey carbon copper grid (200 mesh), the solvent was removed in a vacuum oven during 48 h.

Atomic Force Microscopy (AFM): Was performed under ambient conditions using SPM Nanoscope IIIa multimode working on tapping mode with a RTESPA tip (Veeco) at a working frequency of B235 KHz. Height and phase images were simultaneously obtained. The samples were prepared by drop-casting or spin coating an ethanol solution of the different nanomaterials on freshly cleaved mica. The substrate was dried under ambient conditions for 24 h and, afterwards, in a vacuum oven for 48 h.

X-ray Diffraction (XRD): Was performed with a Panalytical X'Pert PRO diffractometer with Cu tube (λ = 1.5418 Å) in th-2th reflection symmetric mode. The divergence slit was used in automatic mode with 12 mm irradiated constant length. Samples were deposited on "zero background" silicon sample holders and measured in reflection geometry.

X-ray Photoelectron Spectroscopy (XPS): Were performed on a SPECS GmbH (PHOIBOS 150 9MCD) spectrometer operating in the constant analyzer energy mode. A non-monochromatic aluminum X-ray source (1486.61 eV) was used with a power of 200 W and voltage of 12 kV. Pass energies of 75 and 25 eV were used for acquiring both survey and high-resolution spectra, respectively. Survey data were acquired from kinetic energies of 1487–400 eV with an energy step of 1 eV and 100 ms dwell time per point. SpecsLab Version 2.48 software was used for spectrometer control and data handling. The semi-quantitative analyses were performed from the C 1s (284.3 eV) signal. The samples were introduced as pellets of 8 mm diameter.

Synthesis of the Starting CND_{aGlu}: *L*-glutamic acid (1 g) was added into a microwave tube and heated at 210 °C in a microwave reactor for 10 min. A dark brown solid was obtained, which indicates the formation of CND. Then, a few mL of acetone were added, and the dispersion was filtered over a 0.2 µm syringe filter in order to remove the solid byproducts. The collected solution was stored in a freezer in order to precipitate the starting *L*-glutamic acid, which has not reacted. After 24 h. the solution was filtered over a 0.1 µm hydrophilic (PTFE) membrane to remove the excess of *L*- glutamic acid. Once filtered, the collected solution was evaporated under reduced pressure to give rise to the brown solid CND_{aGlu} (0.34 g). FTIR (KBr), ν (cm^{-1}): 1703–1638 (C═O stretching mode), 1500 (C═C stretching mode), 1460–1383 (C—N stretching mode) and 1241–1085 (C—O stretching mode). TGA (N_2 atmosphere): weight loss and temperature desorption (material stability): 90%, 650 °C. XPS (binding Energy, eV)% atomic: C (284.6 eV) = 65.8, O (531.6 eV) = 23.9, N (399.6 eV) = 10.3.

Synthesis of Annealed CND_{aGlu}: In these graphitization experiments, a sample of $CND_{aGlu\ Ini}$ (30 mg) was heated in an oven at different temperatures for 72 h. The temperatures used in each experiment were: 100, 120, 140, 150, 160, 180, 200, and 220 °C generating the corresponding products $CND_{aGlu\,100}$, $CND_{aGlu\,120}$, $CND_{aGlu\,140}$, $CND_{aGlu\,150}$, $CND_{aGlu\,160}$, $CND_{aGlu\,180}$, $CND_{aGlu\,200}$, and $CND_{aGlu\,220}$. The changes observed in comparison with the starting $CND_{aGlu\ Ini}$ were commented and discussed in the "Results and Discussion" section.

Supporting Information

Supporting Information is available from the Wiley Online Library or from the author.

Acknowledgements

Financial support by the Spanish Ministry of Science and Innovation (MICIN) through projects PID2020-115120GB-I00 and PID2020-114653RB-I00/AEI/10.13039/501100011033 and Comunidad de Madrid (CM) through project PR27/21-005 is acknowledged. The authors also thank CM and MICINN for the "(MAD2D-CM)-UCM" project, funded by the Recovery, Transformation and Resilience Plan, and the Next Generation European Union. The collaboration of Prof. Juan Casado in the realization of the Raman investigations is acknowledged.

Conflict of Interest

The authors declare no conflict of interest.

Author Contributions

Nazario Martin: conceptualization (equal); supervision (equal); writing—review editing (equal). **Andres Ferrer-Ruiz**: formal analysis (equal); investigation (equal); writing—original draft (equal). **Laura Rodríguez-Pérez**: formal analysis (equal); investigation (equal); writing—original draft (equal). **María Ángeles Herranz**: conceptualization (equal); supervision (equal); writing—review editing (equal).

Data Availability Statement

The data that support the findings of this study are available from the corresponding author upon reasonable request.

Keywords

carbon dots, *L*-glutamic acid, photoluminescence, post-synthetic graphitization, structural modifications

Received: October 3, 2024
Revised: January 17, 2025
Published online: February 5, 2025

[1] V. Georgaki, J. A. Perman, J. Tucek, R. Zboril, *Chem. Rev.* **2015**, *115*, 4744.
[2] a) Y. Yu, Q. Zeng, S. Tao, C. Xia, C. Liu, P. Liu, B. Yang, *Adv. Sci.* **2023**, *10*, 2207621; b) P. Innocenzi, L. Stagi, *Nano Today* **2023**, *50*, 101837.
[3] Y. Liu, H. Huang, W. Cao, B. Mao, Y. Liu, Z. Kang, *Mater. Chem. Front.* **2020**, *4*, 1586.
[4] a) S. E, Q.-X. Mao, X.-L. Yuan, X.-L. Kong, X.-W. Chen, J.-H. Wang, *Nanoscale* **2018**, *10*, 12788; b) W.-Q. Li, Z. Wang, S. Hao, L. Y. P. Sun, M. Nisic, G. Cheng, C. Zhu, Y. Wan, L. Ha, S.-Y. Zheng, *Nanoscale* **2018**, *10*, 3744; c) S. Chung, R. A. Revia, M. Zhang, *Adv. Mater.* **2021**, *33*, 1904362.
[5] a) Y.-P. Sun, B. Zhou, Y. Lin, W. Wang, K. A. Shiral Fernando, P. Pathak, M. J. Meziani, B. A. Harruff, X. Wang, H. Wang, P. G. Luo, H. Yang, M. Erkan Kose, B. Chen, L. M. Veca, S.-Y. Xie, *J. Am. Chem. Soc.* **2006**, *128*, 7756; b) Y.-P. Sun, L. Yang, *Small Struct.* **2024**, *6*, 2400455.
[6] A. Cayuela, M. L. Soriano, C. Carrillo-Carrión, M. Valcárcel, *Chem. Commun.* **2016**, *52*, 1311.
[7] W. Liang, S. K. Sonkar, D. Saini, K. Sheriff, B. Singh, L. Yang, P. Wang, Y.-P. Sun, *Small* **2023**, *19*, 2206680.
[8] a) T. Yuan, T. Meng, P. He, Y. Shi, Y. Li, X. Li, L. Fan, S. Yang, *J. Mater. Chem. C* **2019**, *7*, 6820; b) D. Qu, Z. Sun, *Mater. Chem. Front.* **2020**, *4*, 400; c) T. C. Wareing, P. Gentile, A. N. Phan, *ACS Nano* **2021**, *15*, 15471.
[9] F. Arcudi, L. Đorđević, *Small* **2023**, *19*, 2300906.
[10] a) L. Tang, R. Ji, X. Cao, J. Lin, H. Jiang, X. Li, K. S. Teng, C. M. Luk, S. Zeng, J. Hao, S. P. Lau, *ACS Nano* **2012**, *6*, 5102; b) F. Arcudi, L. Đorđević, M. Prato, *Acc. Chem. Res.* **2019**, *52*, 2070; c) S. H. Lee, D. Y. Kim, J. Lee, S. B. Lee, H. Han, Y. Y. Kim, S. C. Mun, S. H. Im, T.-H. Kim, O. O. Park, *Nano Lett.* **2019**, *19*, 5437; d) R. Vithalani, D. Patel, C. K. Modi, D. H. Suthar, *J. Mater. Sci.* **2020**, *55*, 8769; e) M. Moniruzzaman, B. Anantha Lakshmi, S. Kim, J. Kim, *Nanoscale* **2020**, *12*, 11947; f) X. Chen, X. Han, C. Zhang, X. Ou, X. Liu, J. Zhang, W. Liu, A. J. Ragauskas, X. Song, Z. Zhang, *Small Struct.* **2024**, *5*, 2300449.
[11] A. T. Krasley, E. Li, J. M. Galeana, C. Bulumulla, A. G. Beyene, G. S. Demirer, *Chem. Rev.* **2024**, *124*, 3085.
[12] a) N. Dhenadhayalan, K.-C. Lin, T. A. Saleh, *Small* **2020**, *16*, 1905767; b) A. Carioscia, E. Cocco, M. E. Casacchia, G. Gentile, M. Mamone, G. Giorgianni, E. Incerto, M. Prato, F. Pesciaioli, G. Filippini, A. Carlone, *ACS Catal.* **2024**, *14*, 13429.
[13] J. Li, X. Zhao, X. Gong, *Small* **2024**, *20*, 2400107.
[14] a) C. Xia, S. Zhu, T. Feng, M. Yang, B. Yang, *Adv. Sci.* **2019**, *6*, 1901316; b) S. Wei, X. Yin, H. Li, X. Du, L. Zhang, Q. Yang, R. Yang, *Chem. Eur. J.* **2020**, *26*, 8129; c) E. A. Stepanidenko, I. A. Arefina, P. D. Khavlyuk, A. Dubavik, K. V. Bogdanov, D. P. Bondarenko, S. A. Cherevkov, E. V. Kundelev, A. V. Fedorov, A. V. Baranov, V. G. Maslov, E. V. Ushakova, A. L. Rogach, *Nanoscale* **2020**, *12*, 602; d) S. Xue, P. Li, L. Sun, L. An, D. Qu, X. Wang, Z. Sun, *Small* **2023**, *19*, 2206180.
[15] a) M. Righetto, F. Carraro, A. Privitera, G. Marafon, A. Moretto, C. Ferrante, *J. Phys. Chem. C* **2020**, *124*, 22314; b) V. Michaud, J. Pracht, F. Schilfarth, C. Damm, B. Platzer, P. Haines, C. Harreiß, D. M. Guldi, E. Spiecker, W. Peukert, *Nanoscale* **2021**, *13*, 13116; c) M. Otten, M. Hildebrandt, R. Kühnemuth, M. Karg, *Langmuir* **2022**, *38*, 6148.
[16] a) J. B. Essner, J. A. Kist, L. Polo-Parada, G. A. Baker, *Chem. Mater.* **2018**, *30*, 1878; b) B. Bartolomei, A. Bogo, F. Amato, G. Ragazzon, M. Prato, *Angew. Chem., Int. Ed.* **2022**, *61*, e202200038; c) A. Roy, C. P. Healey, N. E. Larm, P. Ishtaweera, M. Roca, G. A. Baker, *ACS Nanosci. Au* **2024**, *4*, 176.
[17] a) V. Strauss, J. T. Margraf, C. Dolle, B. Butz, T. J. Nacken, J. Walter, W. Bauer, W. Peukert, E. Spiecker, T. Clark, D. M. Guldi, *J. Am. Chem. Soc.* **2014**, *136*, 17308; b) V. Strauss, J. T. Margraf, K. Dirian, Z. Syrgiannis, M. Prato, C. Wessendorf, A. Hirsch, T. Clark, D. M. Guldi, *Angew. Chem., Int. Ed.* **2015**, *54*, 8292; c) A. Ferrer-Ruiz, T. Scharl, P. Haines, L. Rodríguez-Pérez, A. Cadranel, M. Á. Herranz, D. M. Guldi, N. Martín, *Angew. Chem., Int. Ed.* **2018**, *57*, 1001; d) A. Ferrer-Ruiz, T. Scharl, L. Rodríguez-Perez, A. Cadranel, M. A. Herranz, N. Martín, D. M. Guldi, *J. Am. Chem. Soc.* **2020**, *142*, 20324; e) C. Casadevall, A. Lage, M. Mu, H. F. Greer, D. Antón-García, J. N. Butt, L. J. C. Jeuken, G. W. Watson, M. García-Melchor, E. Reisner, *Nanoscale* **2023**, *15*, 15775.
[18] I. Srivastava, J. S. Khamo, S. Pandit, P. Fathi, X. Huang, A. Cao, R. T. Haasch, S. Nie, K. Zhang, D. Pan, *Adv. Funct. Mater.* **2019**, *29*, 1902466.
[19] D. Mazzier, M. Favaro, S. Agnoli, S. Silvestrini, G. Granozzi, M. Maggini, A. Moretto, *Chem. Commun.* **2014**, *50*, 6592.

[20] H. Moshe, G. Levi, Y. Mastai, *CrystEngComm* **2013**, *15*, 9203.
[21] F. Zhang, X. Feng, Y. Zhang, L. Yan, Y. Yang, X. Liu, *Nanoscale* **2016**, *8*, 8618.
[22] M. Vázquez-Nakagawa, L. Rodríguez-Pérez, M. A. Herranz, N. Martín, *Chem. Commun.* **2016**, *52*, 665.
[23] L. Li, G. Wu, G. Yang, J. Peng, J. Zhao, J.-J. Zhu, *Nanoscale* **2013**, *5*, 4015.
[24] D. García, L. Rodríguez-Pérez, M. A. Herranz, D. Peña, E. Guitián, S. Bailey, Q. Al-Galiby, M. Noori, C. J. Lambert, D. Pérez, N. Martín, *Chem. Commun.* **2016**, *52*, 6677.
[25] T. Scharl, A. Ferrer-Ruiz, A. Saura-Sanmartín, L. Rodríguez-Pérez, N. Martín, M. A. Herranz, D. M. Guldi, *Chem. Commun.* **2019**, *55*, 3223.
[26] S. Zhu, J. Zhang, S. Tang, C. Qiao, L. Wang, H. Wang, X. Liu, B. Li, Y. Li, W. Yu, X. Wang, H. Sun, B. Yang, *Adv. Funct. Mater.* **2012**, *22*, 4732.
[27] a) G. Eda, Y. Lin, C. Mattevi, H. Yamaguchi, H. Chen, I. Chen, C. Chen, M. Chhowalla, *Adv. Mater.* **2010**, *22*, 505; b) G. E. LeCroy, F. Messina, A. Sciortino, C. E. Bunker, P. Wang, K. A. S. Fernando, Y.-P. Sun, *J. Phys. Chem. C* **2017**, *121*, 28180.
[28] N. Dhenadhayalan, K. Lin, R. Suresh, P. Ramamurthy, *J. Phys. Chem. C* **2016**, *120*, 1252.